International Journal of Applied Sciences: Current and Future Research Trends
( IJASCFRT )
**ISSN:** 2790-3990
https://ijascfrtjournal.isrra.org/index.php/Applied_Sciences_Journal

# Desulfurization of Model Oil Fuel with CuW/$TiO_2$−GO through Photocatalytic Oxidation

Mominou Nchare[a*], Moctar Iyami Bintou[b], Abdel Mahlik Mboindi Njifewou[c], Verdo Zizuh Anutebeh[d]

[a,b,c]*Department of Mining & Extractive Metallurgy, School of Geology & Mining Engineering, Meiganga BP 115, Cameroon*

[d]*Faculty of hearth science, Buea, Cameroon*

[a]*Email: nmominou@yahoo.com*

[b]*Email: iyammimoktar@gmail.com*

[c]*Email: mahlickmboindi@gmail.com*

[d]*Email: waneo5@yahoo.com*

**Abstract**

Graphene oxide (GO) was co-modified with copper, tungsten, and titanium oxide. The resulting samples were characterized using the X-ray diffraction (XRD), scanning electron microscopy, X-ray photoelectron spectroscopy, and nitrogen adsorption−desorption techniques. XRD analysis indicated the coexistence of $TiO_2$, CuO, and $WO_3$ in the catalysts. The catalytic performance of the resulting materials in the desulfurization of model oil fuel was evaluated using a photocatalytic reactor. The desulfurization rate, the refined oil yield, and the increase in the octane number of model oil reached 100%, 99.4%, and 1.6 units, respectively, under suitable conditions of a metal content of 10.3%, a metal ratio of 0.7, a reaction temperature of 313K, a reaction time of 1 h, a catalyst/oil ratio of 0.25.

***Keywords:*** Desulfurization; oxidation; photocatalyst; graphene oxide.

## 1. Introduction

The combustion of sulfur-containing fuels releases $SO_x$ emissions, contributing to global warming. Strict regulations have been imposed on the sulfur content of transport fuels to control the SOx emission, and many studies have been focused on the ultra-deep desulfurization technology, which could produce “zero” sulfur fuel.

---

*Received: 5/15/2025*
*Accepted: 7/1/2025*
*Published: 7/14/2025*

---

* *Corresponding author.*

Although conventional hydrodesulfurization (HDS) is widely employed in refineries, it suffers from significant drawbacks, including high hydrogen consumption, extreme operating conditions (>3 MPa, >600 K), and poor efficiency in removing refractory sulfur compounds such as dibenzothiophene (DBT) and benzothiophene (BT) [1–3].

To address these limitations, alternative desulfurization methods have been explored, including biodesulfurization, selective adsorption, oxidative desulfurization (ODS), extractive desulfurization, ionic liquid extraction, alkylation [4–12], sono-hybrid techniques [13], and microbial desulfurization [14]. Among these, adsorptive and oxidative desulfurization are particularly promising due to their mild operating conditions (ambient temperature and pressure). In ODS, sulfur compounds are oxidized to sulfones or sulfoxides [15–19]. Photocatalytic desulfurization has received attention because of using hydrogen peroxide or oxygen as oxidants. Photocatalytic oxidation with $TiO_2$ and indirect photooxidation, which produce oxidants under ultraviolet (UV) irradiation, have been reported. [20,21] However, rapid electron-hole recombination and low oil recovery rates limit the efficiency of these processes. Recent efforts have focused on catalyst modification via doping to reduce bandgap energy or synthesize novel photocatalysts, though not all exhibit high activity [22,23]. $TiO^{2-}$ graphene composites, for instance, demonstrate enhanced electron shuttling and storage properties [24–26]. While such materials have been extensively studied for organic pollutant degradation [27], their application in fuel desulfurization remains underexplored.

In this study, graphene oxide (GO) was co-modified with copper, tungsten, and titanium to enhance photocatalytic selectivity, thermal stability, and charge separation efficiency for desulfurization of model oil fuel. The results demonstrate the potential of this approach for industrial applications.

## 2. Experimental section

### *2.1. Preparation of model oil fuel*

Mercaptan, alkyl sulphide, and thiophene compounds (thiophene, BT, and DBT) were dissolved in the mixture of n-octane (50 mL), benzene (20 mL), and butyl ethylene (30 mL) to obtain the model oil (a sulfur content of 1500 μg/g).

### *2.2. Preparation and Characterization of Catalysts*

$CuW/TiO_2$−GO was synthesized as previously reported [28], titanium tetrachloride (4 g), copper nitrate (2.2 g), ammonium paratungstate (3.8 g), and hydrochloric acid (50 mL) were combined in a 100 mL flask and heated to 313–318 K for 3.5 h. The pH was adjusted to 7 using ammonia solution, followed by impregnation of GO (9 g) at 313 K for 2 h. The material was dried (403 K, 5 h) and calcined (673 K, 3 h). Catalyst crystallinity was analyzed by XRD (D/Max 2500X, Cu Kα radiation) and XPS (PHI-5000C ESCA, Al Kα source). The pore size and volume distribution were tested with nitrogen adsorption−desorption.

### *2.3. Desulfurization Testing*

Reactions were conducted in a photocatalytic reactor equipped with a 100 W mercury lamp (λ = 254 nm). Desulfurization of model oil was carried out in a photocatalytic reactor equipped with mercury lamps. A scheme of the reaction setup is shown in Figure 1. CuW/TiO2−GO (2.5 g) in the photocatalytic reactor was activated at 423 K for 1 h under a nitrogen atmosphere. The photocatalytic reactor was heated gradually to the reaction temperature (293−333 K). Model oil (1 mL/min) and hydrogen peroxide (0.004 mL/min) were preheated to 323 K.

After the reaction, the products were cooled, separated with a gas−liquid separator, and then analyzed by gas chromatography with the atomic emission detector. We calculated the desulfurization rate and refined oil yield as:

$$\text{Desulfurization rate} = (C_1 - C_2)/C_1 \times 100\% \quad (1)$$

$$\text{Refined oil yield} = (M_1 - M_2)/M_1 \times 100\% \quad (2)$$

where $C_1$ and $C_2$ are the sulfur contents of model oil and refined oil, respectively, and $M_1$ and $M_2$ are the masses of model oil and refined oil, respectively.

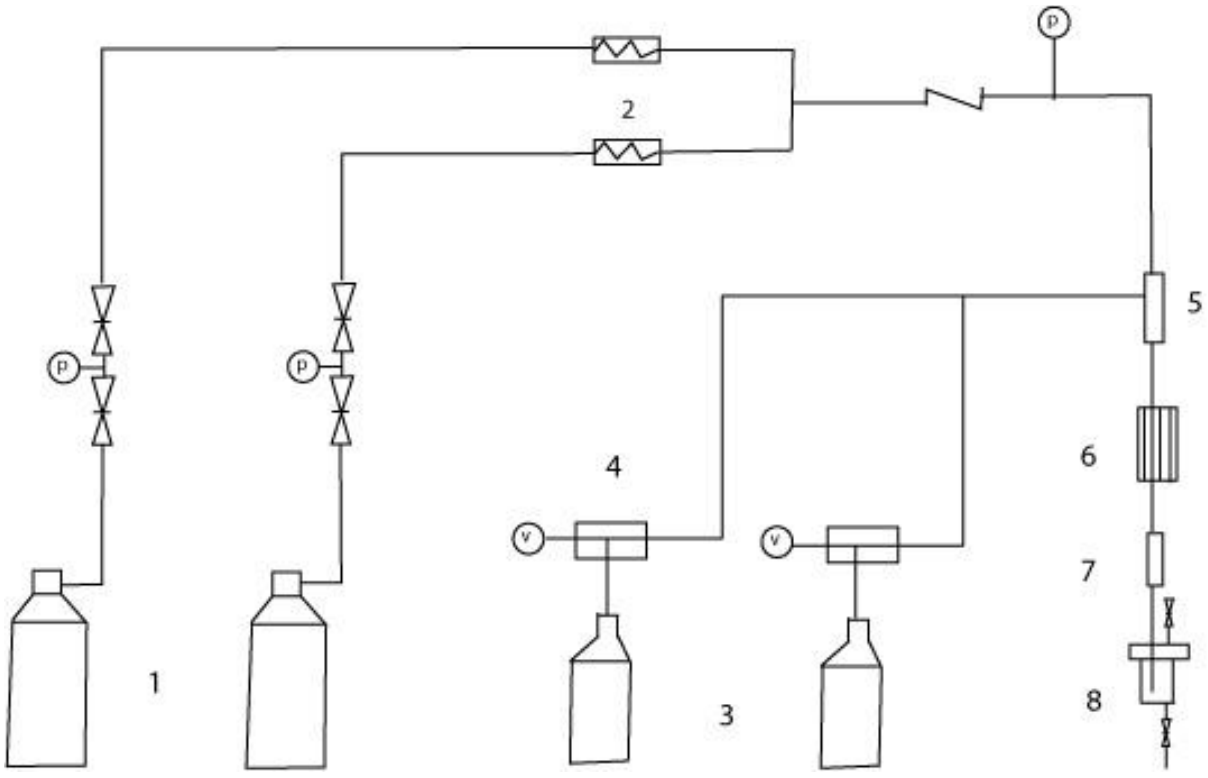


**Figure 1:** Schematic diagram of desulfurization of model oil: (1) air and $N_2$ cylinders, (2) filters, (3) material tank, (4) bumps, (5) mixture, (6) reactor of photocatalytic oxidation, (7) heat exchanger, and (8) gas−liquid separator.

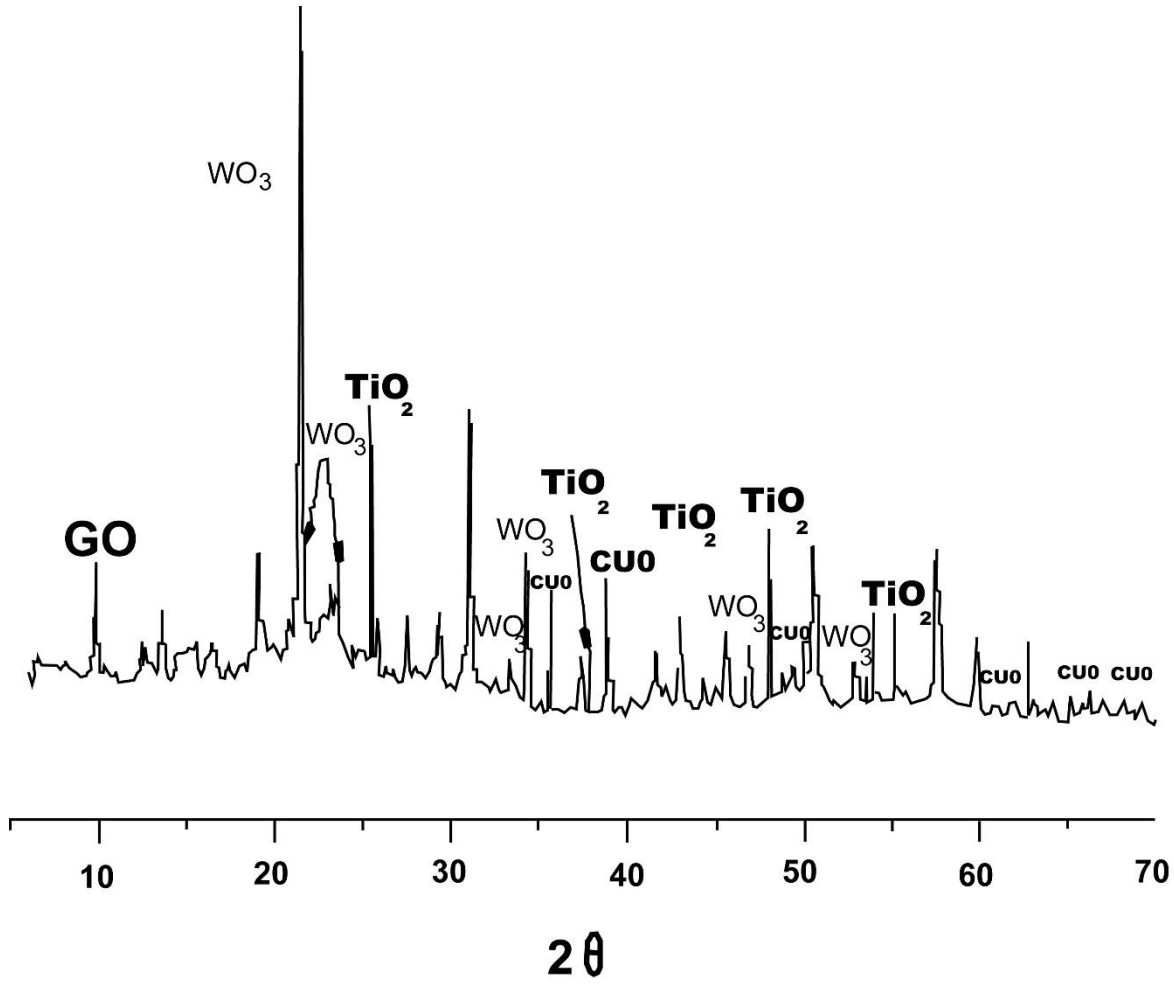


**Figure 2:** XRD patterns of CuW/TiO2−GO.

As shown in Figure 3a, when $P/P_0$ was lower than 0.43, the adsorption capacity increased with the increase of the relative pressure ($P/P_0$), indicating that $CuW/TiO_2$−GO possessed a certain amount of micropores. The curves of desorption and adsorption no longer overlapped when $P/P_0$ increased further, and there was a clear hysteresis loop, which indicated that the catalyst possessed a large number of mesopores. While $P/P_0$ was close to 1, the adsorption capacity of $CuW/TiO_2$−GO was increased rapidly and did not reach saturation, which indicated that the catalysts also contained a small part of macropores. $CuW/TiO_2$−GO had a wide distribution of the pore size, as shown in Figure 3b; the majority of holes was mesopores (2−25 nm), besides a small number of micropores. The average pore size and pore volume were 7.02 nm and 1.34 cm3/g, respectively. The peaks of O 1s, C 1s, W 4f, Cu 2p, and Ti 2p were marked in the overview XPS spectra of CuW/TiO2−GO (Figure 4).

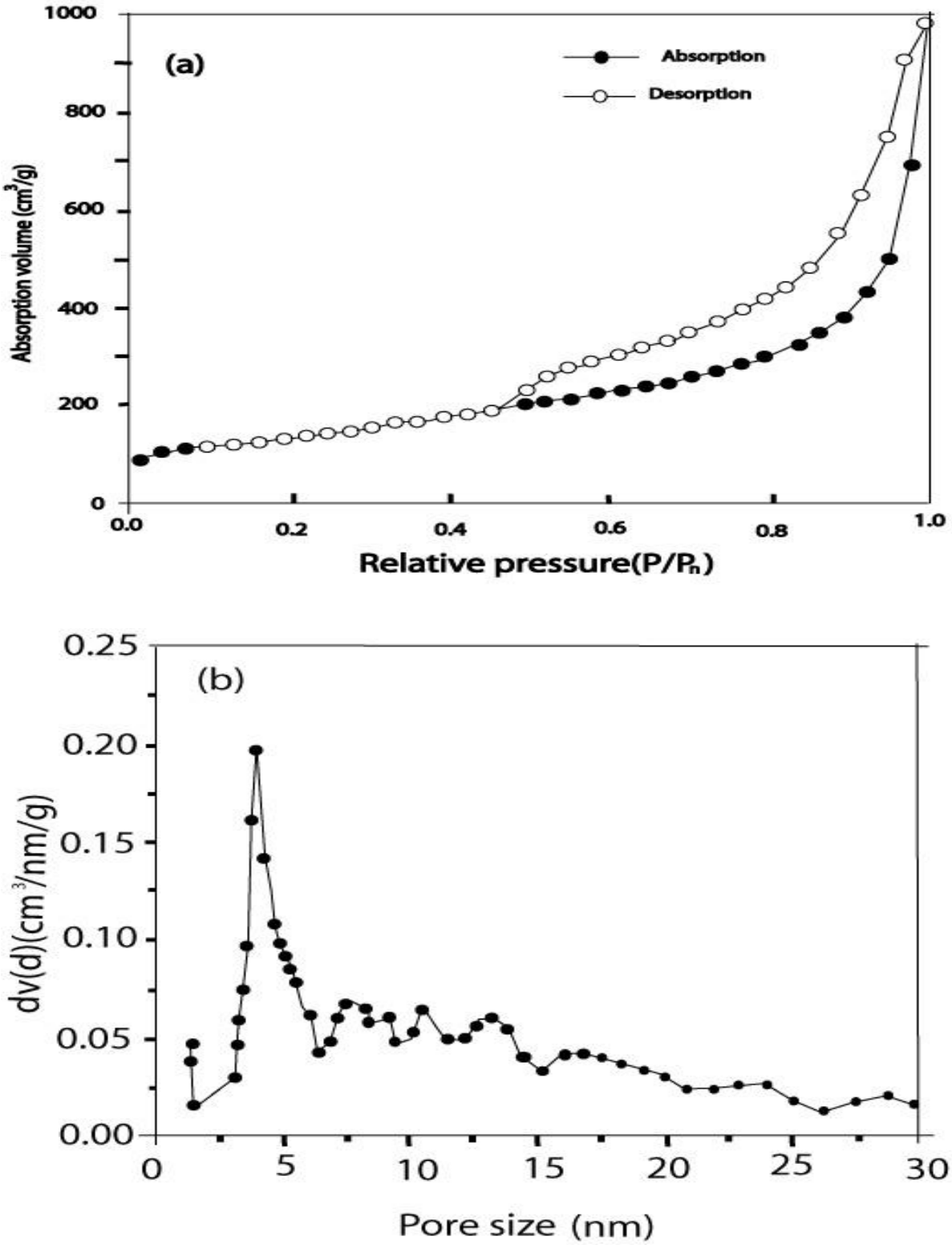


**Figure 3:** (a) Nitrogen physisorption isotherms and (b) pore size distribution curve of CuW/$TiO_2$−GO.

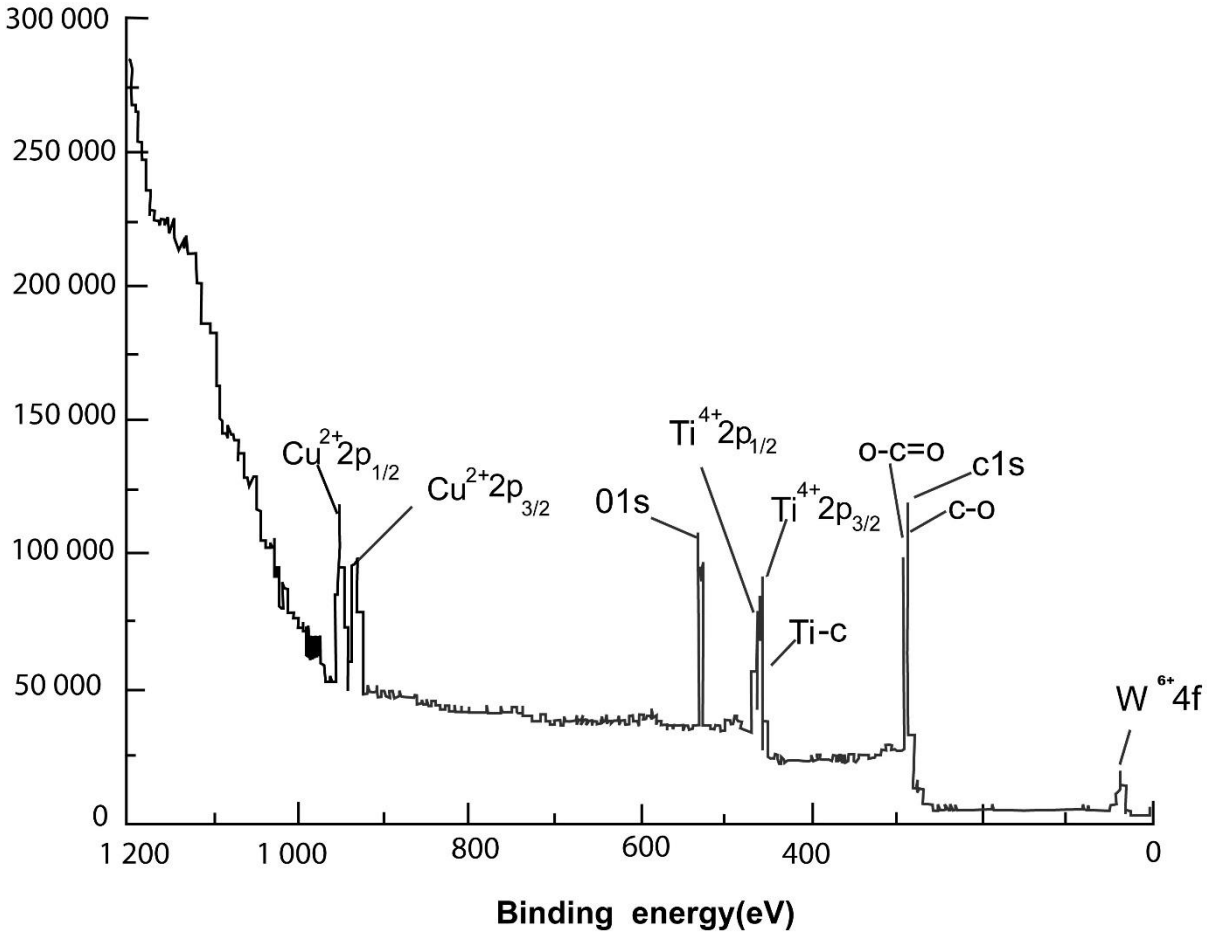


**Figure 4:** XPS of $CuW/TiO_2$−GO.

The C 1s XPS spectra of GO at 284.7, 287.0, and 288.9 eV were assigned to $sp^2$ carbon components, C−O single bond components, and C = O double bond components, respectively.[29] The peaks at 529.6 and 530.5 eV were credited to O 1s. The XPS signal of W 4f at 35.7 eV was ascribed to $W^{6+}$. The XPS spectra of Ti 2p and Cu 2p at 464.7 eV (Ti $2p^{1/2}$),459 eV (Ti $2p^{3/2}$), 953.7 eV (Cu $2p^{1/2}$), and 934.6 eV ($Cu2p^{3/2}$) were attributed to $Ti^{4+}$ and $Cu^{2+}$, respectively.

### *3.2. Effects of the Catalyst Metal Content on the Desulfurization Rate*

Increasing the content of copper, tungsten, and titanium species can improve the photocatalytic activity of $CuW/TiO_2$−GO for the desulfurization of model oil. The desulfurization rate increases rapidly and reaches the maximum when the metal ratio increased from 0 to 0.7 (Figure 5a), whereas a gradual decrease in the desulfurization rate is observed after the ratio increased higher than 0.7. The highest desulfurization rate was 98% at a 10.3% Cu−W−Ti content and a CuW (Cu/W = 0.7:1) /Ti ratio of 0.7 (Figure 5b).

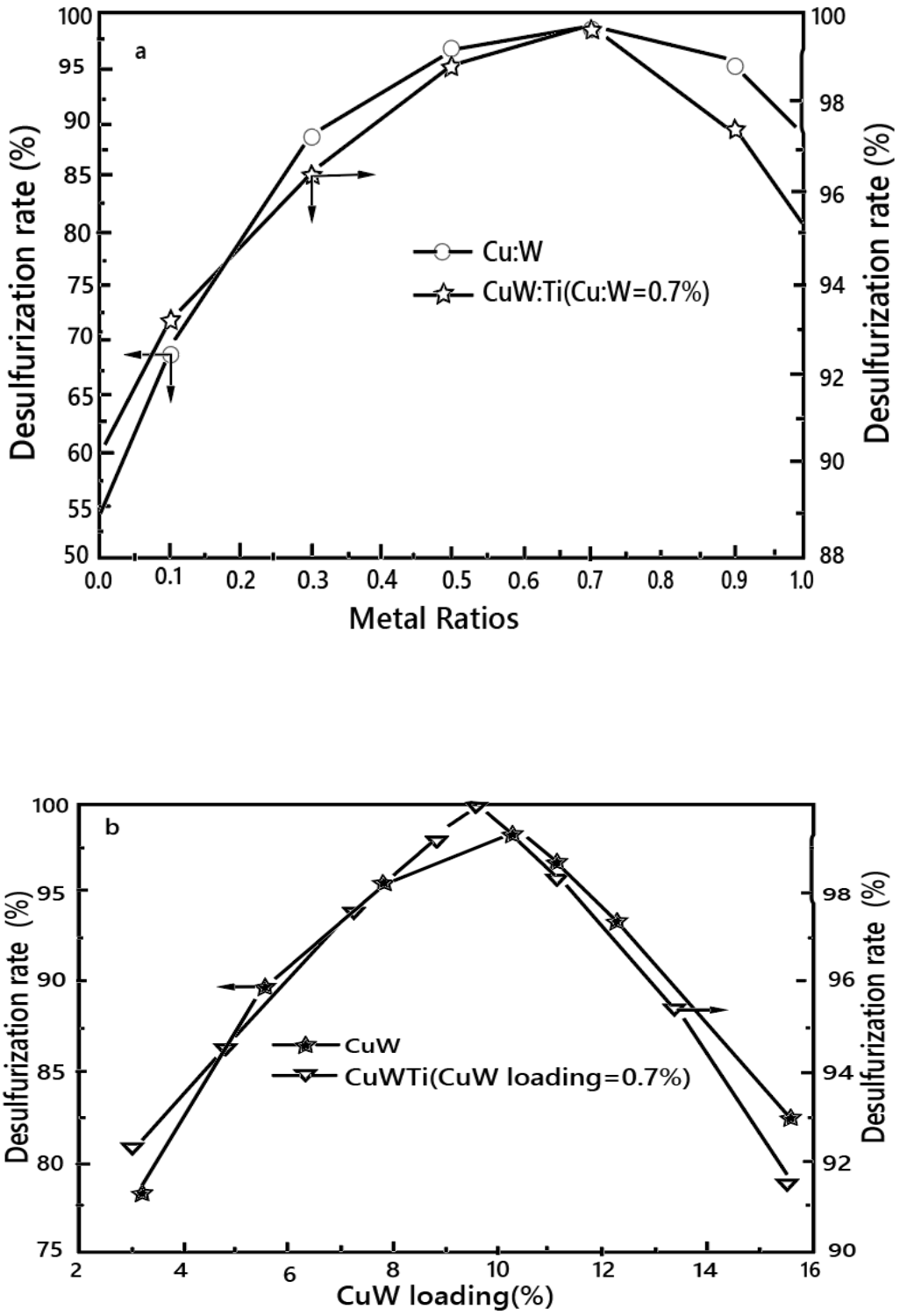


**Figure 5:** Effects of the metal content on the desulfurization rate of model oil (with the oxidant percent of 0.5%, the catalyst/oil weight ratio of 0.25, the reaction time of 1 h, and the temperature of 313 $^{0}$K.

The desulfurization rate decreases with a further increase in the metal content. Catalysts to which only Cu species were added showed negligible activity for desulfurization of model oil, whereas the addition of copper, tungsten, and titanium species increased the activity. Therefore, the variation of the desulfurization activity should be related to the types and dispersion of metals on the catalyst surface. The decrease in the desulfurization rate at higher metal content can be ascribed to the decreasing accessibility of active sites. Owing to the presence of different active sites, $CuW/TiO_2$−GO is active not only for the removal of thiophene and its derivatives but also for the removal of other sulfur compounds. First because the photogenerated electrons had a tendency to transfer from p-CuO to n-$WO_3$ or n-$TiO_2$ and the holes had an opposite tendency as a result of n−p junctions between p-CuO and n-$WO_3$ (or n-$TiO_2$). Second, the GO surface could decrease the recombination rate of photogenerated holes and electrons, because it acted as electron-trapping sites to trap the electrons and transfer them to hydrogen peroxide adsorbed on the CuW/TiO2−GO surface. [30−39]

### *3.3. Effects of the Temperature on the Desulfurization Rate*

The desulfurization of model oil with $CuW/TiO_2$−GO was carried out at temperatures from 293 to 333K.When the reaction temperature was increased from 293 to 313 K, the desulfurization rate of mercaptan, alkyl sulphide, and thiophene compounds gradually increased and reached a maximum. The desulfurization rate gradually decreased as the temperature was increased further (Figure 6). The increase in the temperature had an advantage to not only the desulfurization of model oil but also the decomposition of oxidants. The desulfurization rate reaches a maximum at 313K. The lower desulfurization rate at a higher temperature might be due to the rapid decomposition of $H_2O_2$.

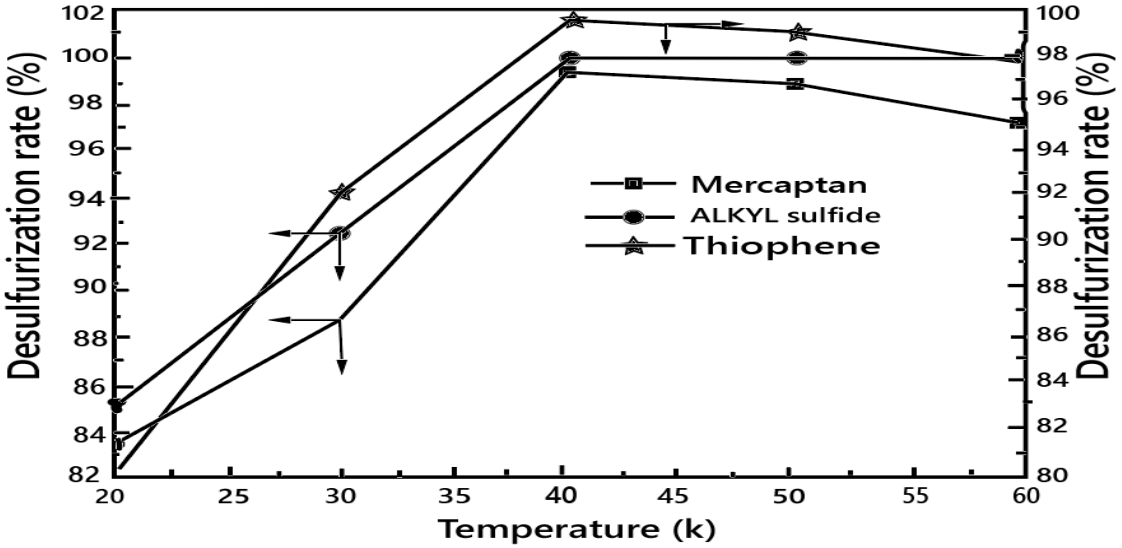


**Figure 6:** Effects of the temperature on the desulfurization rates of model oil (with the oxidant percent of 0.5%, the catalyst/oil weight ratio of 0.25, the metal content of 10.3%, the metal weight ratio of 0.7, and the reaction time of 1h.

### *3.4. Effects of the Catalyst/ Oil Ratio on the Desulfurization Rate*

A consistent increase in the desulfurization rate of mercaptan, alkyl sulphide, and thiophene compounds increased gradually, and reached a plateau with increasing the catalyst/oil ratios (Figure 7).

The desulfurization rate of mercaptan, alkyl sulphide, and thiophene compounds reached the maximum desulfurization rates of 99.8, 100, and 99.9%, respectively, when the ratio was 0.25. Although the higher catalyst/oil ratios produced the more active sites of photocatalytic desulfurization, the turbidity of the reaction solution was increased as a result of the increase in the amount of catalyst. The catalyst/Oil ratio of 0.25 was favorable for the desulfurization of model oil.

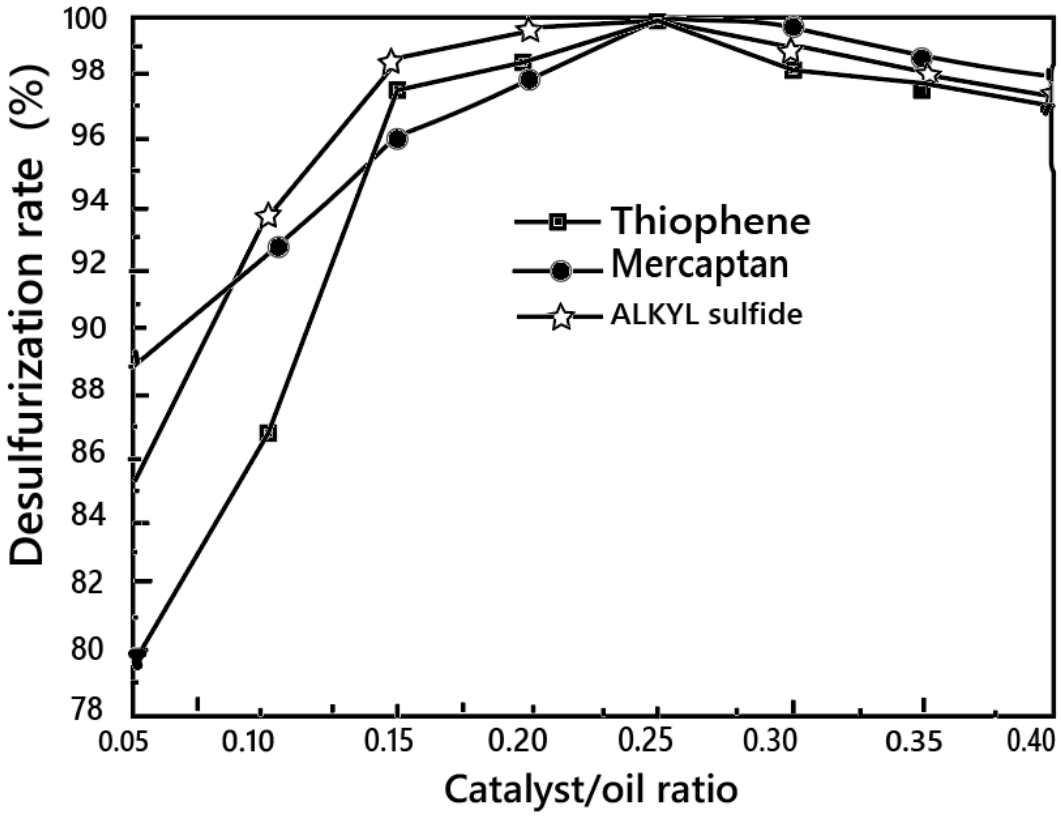


**Figure 7:** Effects of the catalyst/ oil ratios on the desulfurization rates of model oil (with the oxidant percent of 0.5%, the metal content of 10.3%, the metal weight ratio of 0.7, the reaction time of 1h, and the temperature of 313 K.

### *3.5. Effects of the Reaction Time on the Desulfurization Rate*

The desulfurization rate gradually increased and reached a plateau as the reaction time was increased (Figure 8). The desulfurization rates of mercaptan, alkyl sulphide, and thiophene compounds reached the maximum of 98% at the reaction time of 1 h. The contact time between reactants and active sites was shortened with decreasing

the reaction time. On the contrary, the change of the desulfurization rate of model oil was slow because of decreasing the concentration of the reactants with increasing the reaction time. The reaction time of 1 h was suitable for the desulfurization of modele oil.

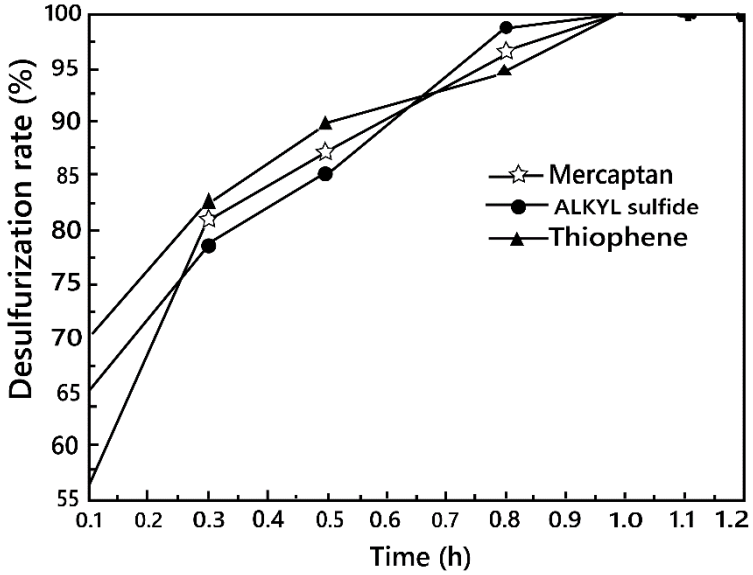


**Figure 8:** Effects of the time on the desulfurization rates of modele oil (with the oxidant percent of 0.5%, the metal content of 10.3%, the metal weight ratio of 0.7, the catalyst/oil ratio of 0.25, the reaction time of 1 h, and the temperature of 313 K.

### *3.6. Catalyst Recycle*

The recycle of $CuW/TiO_2$−GO catalysts for desulfurization of modele oil was investigated. The sulfur content of modele oil was decreased from 1500 to 900 μg/g using the catalyst of $CuW/TiO_2$−GO under the suitable conditions.

## 4. Conclusion

$CuW/TiO_2$−GO exhibited exceptional photocatalytic activity for model oil desulfurization, achieving 98% sulfur removal and 99.4% oil yield under mild conditions. The catalyst's dual function (oxidation and cetane number enhancement) distinguishes it from conventional systems. Future work will focus on industrial-scale longevity and regeneration protocols. The sulfur compound content of modele oil was reduced from 1500 to 6.3 μg/g. Future work will focus on industrial-scale longevity and regeneration protocols.

## Acknowledgements

Special thanks to professor Wang Lei and Dr Li Hong for the collaboration during the last two decades

**References**


[1]. Bhasarkar, J. B.; Chakma, S.; Moholkar, V. S. Mechanistic Features of Oxidative Desulfurization Using Sono-Fenton-Peracetic Acid (Ultrasound /Fe2+-$CH_3COOH$-$H_2O_2$) System. Ind. Eng. Chem.Res. 2013, 52, 9038−9047.

[2]. Wang, L.; Cai, H.; Li, S.; Mominou, N. Ultra-deep Removal of Thiophene Compounds in Diesel Oil over Catalyst $TiO_2$/Ni-ZSM-5 Assisted by Ultraviolet Irradiating. Fuel 2013, 105, 752−756.

[3]. Lorencon, E.; Alves, D. C. B.; Krambrock, K.; Ávila, E. S.; Resende, R. R.; Ferlauto, A. S.; Lago, R. M. Oxidative Desulfurization of Dibenzothiophene over Titanate Nanotubes. Fuel 2014, 132, 53−61.

[4]. Julião, D.; Gomes, A. C.; Pillinger, M.; Cunha-Silva, L.; de Castro, B.; Gonçalves, I. S.; Balula, S. S. Desulfurization of Model Diesel by Extraction/Oxidation Using a Zinc-substituted Polyoxometalate as Catalyst under Homogeneous and Heterogeneous (MIL-101(Cr) Encapsulated) Conditions. Fuel Process. Technol. 2015, 131, 78−86.

[5]. Shu, C.; Sun, T.; Zhang, H.; Jia, J.; Lou, Z. A Novel Process for Gasoline Desulfurization Based on Extraction with Ionic Liquids and Reduction by Sodium Borohydride. Fuel 2014, 121, 72−78.

[6]. Tao, H.; Nakazato, T.; Sato, S. Ultra-deep Desulfurization of Kerosene Based on Selective Photooxidation and Adsorption. Fuel 2009, 88, 1961−1969.

[7]. Ahmed, I.; Jhung, S. H. Adsorptive Desulfurization and Denitrogenation Using Metal-organic Frameworks. J. Hazard. Mater.2016, 301, 259−276.

[8]. Jaimes, L.; Badillo, M.; de Lasa, H. FCC Gasoline Desulfurization Using a ZSM-5 Catalyst Interactive Effects of Sulfur Containing Species and Gasoline Components. Fuel 2011, 90, 2016−2025.

[9]. Zhang, C.; Pan, X.; Wang, F.; Liu, X. Extraction-oxidation Desulfurization by Pyridinium-based Task-specific Ionic Liquids. Fuel 2012, 102, 580−584.

[10]. Shangguan, J.; Zhao, Y.; Fan, H.; Liang, L.; Shen, F.; Miao, M. Desulfurization Behavior of Zinc Oxide Based Sorbent Modified by the Combination of $Al_2O_3$ and $K_2CO_3$. Fuel 2013, 108, 80−84.

[11]. Gupta, M.; He, J.; Nguyen, T.; Petzold, F.; Fonseca, D.; Jasinski, J. B.; Sunkara, M. K. Nanowire Catalysts for Ultra-deep Hydrodesulfurization and Aromatic Hydrogenation. Appl. Catal., B 2016, 180, 246−254.

[12]. Yu, S.; Pan, F.; Yang, S.; Ding, H.; Jiang, Z.; Wang, B.; Li, Z.; Cao, X. Enhanced Pervaporation Performance of MIL-101 (Cr) Filled Polysiloxane Hybrid Membranes in Desulfurization of Model Gasoline. Chem. Eng. Sci. 2015, 135, 479−488.

[13]. Bhasarkar, J. B.; Chakma, S.; Moholkar, V. S. Investigations in Physical Mechanism of the Oxidative Desulfurization Process Assisted Simultaneously by Phase Transfer Agent and Ultrasound. Ultrason. Sonochem. 2015, 24, 98−106.

[14]. Bhasarkar, J. B.; Dikshit, P. K.; Moholkar, V. S. Ultrasound Assisted Biodesulfurization of Liquid Fuel using Free and Immobilized Cells of Rhodococcus Rhodochrous MTCC 3552: A Mechanistic Investigation. Bioresour. Technol. 2015, 187, 369−378.

[15]. Zhang, K.; Liu, Y.; Tian, S.; Zhao, E.; Zhang, J.; Liu, C. Preparation of Bifunctional NiPb/ZnO-diatomite-ZSM-5 Catalyst and Its Reactive Adsorption Desulfurization Coupling Aromatization Performance in FCC Gasoline Upgrad ing Process. Fuel 2013, 104, 201−207.

[16]. Al-Bogami, S. A.; de Lasa, H. I. Catalytic Conversion of Benzothiophene over a H-ZSM5 Based Catalyst. Fuel 2013, 108, 490−501.

[17]. Wang, R.; Wan, J.; Li, Y.; Sun, H. A Further Catalysis Mechanism Study on Amberlyst 35 Resins Application in Alkylation Desulfurization of Gasoline. Chem. Eng. Sci. 2015, 137, 59−68.

[18]. Gu, Q.; Zhu, W.; Xun, S.; Chang, Y.; Xiong, J.; Zhang, M.; Jiang, W.; Zhu, F.; Li, H. Preparation of Highly Dispersed Tungsten Species within Mesoporous Silica by Ionic Liquid and Their Enhanced Catalytic Activity for Oxidative Desulfurization. Fuel 2014, 117, 667−673.

[19]. Shu, C.; Sun, T.; Jia, J.; Lou, Z. Mild Process for Reductive Desulfurization of Diesel Fuel Using Sodium Borohydride in Situ Generated via Sodium Metaborate Electroreduction. Ind. Eng. Chem.Res. 2013, 52, 7660−7667.

[20]. Zheng, D.; Zhu, W.; Xun, S.; Zhou, M.; Zhang, M.; Jiang, W.; Qin, Y.; Li, H. Deep Oxidative Desulfurization of Dibenzothiophene Using Low-Temperature-Mediated Titanium Dioxide Catalyst in Ionic Liquids. Fuel 2015, 159, 446−453.

[21]. Wang, L.; Shen, B.; Li, S. Model of Fluidized Catalytically Cracked (FCC) Gasoline Photochemical Desulfurization Reactor. Energy Fuels 2006, 20, 1287−1293.

[22]. Chakma, S.; Moholkar, V. S. Sonochemical Synthesis of Mesoporous ZrFe2O5 and its Application for Degradation of Recalcitrant Pollutants. RSC Adv. 2015, 5, 53529−53542.

[23]. Chakma, S.; Moholkar, V. S. Investigation in Mechanistic Issues of Sonocatalysis and Sonophotocatalysis using Pure and Doped Photocatalysts. Ultrason. Sonochem. 2015, 22, 287−299.

[24]. Mohd Zaid, H. F.; Chong, F. K.; Abdul Mutalib, M. I. Photooxidative-Extractive Deep Desulfurization of Diesel Using Cu-Fe/TiO2 and Eutectic Ionic Liquid. Fuel 2015, 156, 54−62.

[25]. Lü, X.; Yang, W.; Quan, Z.; Lin, T.; Bai, L.; Wang, L.; Huang, F.; Zhao, Y. Enhanced Electron Transport in Nb-Doped TiO2 Nanoparticles via Pressure-Induced Phase Transitions. J. Am. Chem. Soc. 2014, 136, 419−426.

[26]. Williams, G.; Seger, B.; Kamat, P. V. $TiO_2$-graphene Nanocomposites UV Assisted Photocatalytic Reduction of Graphene

[27]. Lei, M.; Wang, N.; Zhu, L.; Xie, C.; Tang, H. A Peculiar Mechanism for the Photocatalytic Reduction of Decabromodiphenyl Ether over Reduced Graphene Oxide-TiO2 Photocatalyst. Chem. Eng. J. 2014, 241, 207−215.

[28]. Xiang, Q.; Yu, J.; Jaroniec, M. Graphene Based Semiconductor Photocatalysts. Chem. Soc. Rev. 2012, 41, 782−796.

[29]. Park, S.; Lee, K.-S.; Bozoklu, G.; Cai, W.; Nguyen, S. T.; Ruoff, R. S. Graphene Oxide Papers Modified by Divalentions-Enhancing Mechanical Properties via Chemical Cross-linking. ACS Nano 2008, 2,572−578.

[30]. Irie, H.; Kamiya, K.; Shibanuma, T.; Miura, S.; Tryk, D. A.; Yokoyama, T.; Hashimoto, K. Visible Light-Sensitive Cu(II)-Grafted $TiO_2$ Photocatalysts: Activities and X-ray Absorption Fine Structure Analyses. J. Phys. Chem. C 2009, 113, 10761−10766.

[31]. Qiu, X.; Miyauchi, M.; Yu, H.; Irie, H.; Hashimoto, K. Visible Light Driven Cu(II)-(Sr1-yNay) (Ti1-xMox)$O_3$ Photocatalysts Based on Conduction Band Control and Surface Ion Modification. J. Am. Chem. Soc. 2010, 132, 15259−15267.

[32]. Yu, H.; Irie, H.; Hashimoto, K. Conduction Band Energy Level Control of Titanium Dioxide: Toward an Efficient Visible-Light-Sensitive Photocatalyst. J. Am. Chem. Soc. 2010, 132, 6898−6899.

[33]. Leflaive, P.; Lemberton, J. L.; Pérot, G.; Mirgain, C.; Carriat, J.Y.; Colin, J. M. On the Origin of Sulfur Impurities in Fluid Catalytic Cracking Gasoline-Reactivity of Thiophene Derivatives and of Their Possible Precursors under FCC Conditions. Appl. Catal., A 2002, 227, 201−215.

[34]. Lee, M.; Yong, K. Highly Efficient Visible Light Photocatalysis of Novel CuS/ZnO Heterostructure Nanowire Arrays. Nanotechnology 2012, 23, 4014−4019.

[35]. Jing, L.; Zhou, W.; Tian, G.; Fu, H. Surface Tuning for Oxide based Nanomaterials as Efficient Photocatalyst. Chem. Soc. Rev. 2013, 42, 9509−9549.

[36]. Rodríguez-Cabo, B.; Rodríguez, H.; Rodil, E.; Arce, A.; Soto, A. Extractive and Oxidative-extractive Desulfurization of Fuels with Ionic Liquids. Fuel 2014, 117, 882−889.

[37]. Shand, M.; Anderson, J. A. Aqueous Phase Photocatalytic Nitrate Destruction Using Titania Based Materials: Routes to Enhanced Performance and Prospects for Visible Light Activation. Catal. Sci. Technol. 2013, 3, 879−899.

[38]. Osterloh, F. E. Inorganic Nanostructures for Photoelectrochemical and Photo -catalytic Water Splitting. Chem. Soc. Rev. 2013, 42, 2294−2320.

[39]. Xiao, J.; Wu, L.; Wu, Y.; Liu, B.; Dai, L.; Li, Z.; Xia, Q.; Xi, H. Effect of Gasoline Composition on Oxidative Desulfurization Using a Phosphotungstic Acid/ Activated Carbon Catalyst with Hydrogen Peroxide. Appl. Energy 2014, 113, 78−85.